Improved Fault Location on Distribution Feeders Based on Matching During-Fault Voltage Sags

Rodrigo Aparecido Fernandes Pereira, Luis Gustavo Wesz da Silva, Mladen Kezunovic, *Fellow, IEEE*, and José Roberto Sanches Mantovani, *Member, IEEE*

Abstract—A fault location algorithm for distribution feeders based on matching during-fault voltage sags is presented. The basic principle of the algorithm is based on the fact that when a fault occurs on the feeder, voltage sags propagate presenting different characteristics for each feeder node. Knowing the voltage sag characteristics, it is possible to locate the faulty node or the faulty area of the feeder. This voltage-based approach ensures the efficiency and robustness of the algorithm, which provides suitable and accurate results. An overhead, three-phase, three-wire, 13.8 kV, 134-node, real-life feeder model is used to evaluate the algorithm. Test results show that the algorithm is quite suitable due to not only the faulted point being located, but also a faulted area being identified providing important information to direct the maintenance crew seeking to repair any fault inflicted damage.

Index Terms—Fault location, power distribution, voltage measurement, voltage sags.

I. INTRODUCTION

FAULTS on distribution feeders cause the protection system to react interrupting the power supply. Generally, severe weather conditions such as lightning and thunderstorms, animals or trees touching energized parts of the network, as well as aging and inadequate maintenance of network components, are the main fault causes [1]. Usually, pinpointing the fault or the faulted area is a hard task to be accomplished. This may causes degradation of reliability indices, which depend on the interruptions duration, such as: system average interruption duration index (SAIDI), customer average interruption duration index (CAIDI) and customer total average interruption duration index (CTAIDI) [1].

In order to pinpoint the fault, some proposed fault location algorithms are based on phasors of fundamental frequency of voltages and currents measured at the feeder root node, as well as apparent impedance computation [2]–[5]. A technique based on

the integration of information from fault indicators placed along the feeder, computation of apparent impedance using voltage and current phasors measured at the feeder root node along with statistical frequency of fault occurrence on the feeder is proposed in [6]. An iterative fault location algorithm based on superimposed components of voltages and currents is proposed in [7]. Iterative algorithms that compute the fault distance based on fundamental frequency phasors of voltages and currents measured at the feeder root node, as well as diagnosis and analysis of waveforms matching along with rejected loads after the fault clearing are proposed in [8]–[10]. A program, which is for the analysis of electric power systems in association with methods for database search, pattern recognition techniques, usage of during-fault voltage magnitudes and phase angles measured at the feeder root node, is proposed in [11]. Reference [12] presents an algorithm for fault location in automated distribution systems. This algorithm uses the voltages and currents recorded at the sending and receiving nodes of all considered line sections. A methodology employing voltage and current measurements at several points along the feeder, oriented graph theory, and analysis of electric circuits is presented in [13]. Reference [14] presents a methodology based on information from fault detectors placed along the feeder and fuzzy logic to handle the information. A fault locator based on fault generated high frequency noise signal is proposed in [15]. References [16] and [17] present fault location techniques for transmission lines using measurements of voltages. Reference [18] presents a technique for locating single-line-to-ground faults on distribution feeders by using fault simulations and voltage matching. The usage of this technique is straightforward for locating single-line-to-ground faults, and its efficiency is demonstrated by the presented results. The applicability of this technique is not so trivial for locating other fault types, such as three-phase or line-to-line faults, due to the complexity of calculating the fault resistances required for the fault location process.

The fault location algorithm proposed in this paper is based on matching during-fault voltage sag magnitudes. Its applicability is straightforward for any fault types because no fault impedance is required in the fault modeling used in the algorithm. In order to locate a fault, the algorithm uses the pre- and during-fault fundamental frequency phasors of voltages and currents recorded at the feeder root node, the during-fault voltage sag magnitudes measured at some remote nodes along the feeder, as well as a feeder database containing parameters such as feeder topology, line section impedance and nominal power of the transformer connected to the feeder. Section II presents a brief fault location and distribution network background. The fault location algorithm is presented in Section III.

The main requirements of the algorithm are presented in Section IV. In order to assess the efficiency and robustness of the algorithm, results and analyses of simulations performed for an overhead, three-phase, three-wire, 13.8 kV, 134-node, real-life feeder are presented in Sections V and VI. Conclusions are presented in Section VII.

II. Fault Location and Distribution Network Background

One way that can be used by utilities to minimize the degradation of reliability indices is to deploy fast and efficient algorithms and techniques for fault location. A procedure widely used by electric utilities is the trial and error fault location method. Based on the knowledge of operators, several opening and closing operations of reconfiguration switches are performed for locating and isolating the fault. In most cases, the trial and error based-method is a very lengthy process resulting in long outages. After electric utilities have introduced the call centers, the trial and error procedure for fault location was improved based on customer complaints affected by outages. Even with this new information received at the call centers, more improvements are required to enhance the fault location procedure. Due to this necessity and supported by the fast evolution of the technology for acquisition, processing, and transmission of signal measurements along feeders, several algorithms and techniques for fault location on distribution feeders have been proposed [2]–[15], [18].

Generally, overhead distribution networks are nontransposed and the line impedances are unbalanced. They are typically configured in radial topology with several line sections having three, two or single-phase laterals, different load types, and low X/R ratio. An accurate fault location technique must be able to handle in an efficient way such networks.

III. Basic Algorithm for Fault Location

Aiming to meet these mentioned requirements, the proposed algorithm was developed based on the Backward/Forward Sweep Load Flow method [19] along with voltage sag measurements at some feeder nodes. The Backward/Forward Sweep Load Flow method, which calculates the branch currents in one backward sweep (from end branches to substation) and the nodal voltages in one forward sweep (from substation to last nodes), was chosen because it is suitable and efficient to analyze distribution networks. The basic principle of the algorithm is that, when a fault occurs in the feeder, voltage sags propagate presenting different magnitudes and phase angle for each feeder node. The different voltage sags experienced by each feeder node are allowing the algorithm to use sparse voltage measurements from a reduced set of measurement devices strategically placed along the feeder providing sufficient data for accurate results.

The steps of the fault location algorithm are as follows.

Step 1) Read the phasors of voltages (pre- and during-fault) and currents (pre- and during-fault) for the root node, the voltage sag magnitudes measured for some nodes along the feeder, as well as the faulted phase and fault type.

Step 2) Collect the feeder data into a database and make it available for further computations.

Step 3) Select the load model to be used and set the related event scenarios.

Step 4) Estimate the power rating for each feeder transformer.

Step 5) Attribute voltages at all nodes based on the during-fault voltages measured at the feeder root.

Step 6) Calculate the fault current.

Step 7) Inject the fault current at the analyzed node.

Step 8) Execute the during-fault load flow.

Step 9) Check whether the calculated currents for the root node are equal to the measured current for this node. If not, go to Step 6). If yes, calculate the mismatches between measured and calculated voltages for the measurement nodes.

Step 10) Change the analyzed node and go to Step 5), repeating the process until the last node is analyzed.

Step 11) Considering the fault at each analyzed node, calculate the fault location indices [i.e., the difference between the biggest and the smallest voltage mismatches (Step 9)] for all measurement nodes.

Step 12) Classify in a decreasing ranking the fault location indices in order to identify the likely faulted node.

Step 13) Select as the faulted node the one having the biggest fault location index (Step 12).

Section IV clarifies how each of the mentioned steps should be carried out in order to accomplish the fault location algorithm.

IV. Main Requirements of the Algorithm

A. Voltage and Current Measurements on the Feeder

The proposed algorithm uses voltage and current measurements at the feeder root node as well as sparse voltage measurements at some nodes along the feeder. Pre- and during-fault voltage and current phasors must be recorded at the feeder root node. Pre-fault phasor quantities are used in the computation of the total pre-fault complex power of the feeder. This power is used in the distribution transformer power rating estimation. During-fault phasor quantities are used in the fault location procedure. Sparse measurements at some feeder nodes provide the during-fault voltage sag magnitudes used by the algorithm in order to find the faulted point.

Since the algorithm requires the voltage and current phasors recorded at the feeder root node, these quantities need to be recorded in a time-synchronized way. Additionally, the algorithm requires the voltage sag magnitudes recorded at sparse measurement nodes, but these recorded quantities neither need to be synchronized among themselves nor with the quantities recorded at the feeder root node, which may be synchronized using GPS means. However, it is required that the quantities delivered to the algorithm be recorded for the same fault event. For this purpose, a mobile telephone network can be used to provide the time stamp for the sampled voltage sag magnitudes and to transmit the recorded quantities, since they will be transmitted to a central point for the algorithm processing when a fault occurs. The recorded quantities are processed at the measurement site
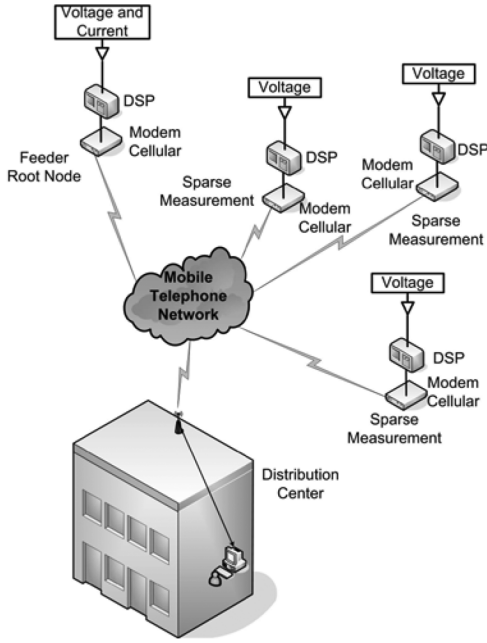
Fig. 1.   Basic architecture of the fault locator.

before the transmission. Additionally, the sparse measurement devices are triggered to record when the voltage drops below a pre-established threshold value. Similarly, the measurement device placed at the feeder root node is triggered to record when the current rises above a pre-established threshold value. Fig. 1 illustrates in a simplified way the data recording architecture for a fault locator by using the proposed algorithm.

B. Feeder Database

The feeder database contains topological information, such as the line section length and places where transformers and protective devices are installed on the feeder as well as electric parameters, such as line section impedances, transformer nominal power and nominal voltage.

C. Load Modeling

Usually, loads connected at a distribution feeder are specified based on their complex power demand. These loads can be three, two or single-phase. In this paper, the load models with constant power, constant current and constant impedance are defined as follows:

$$\mathbf{S} = \mathbf{S}^{nom} \left(\frac{|\mathbf{V}|}{|\mathbf{V}_{nom}|} \right)^{q} \tag{1}$$

where

$\mathbf{S}^{nom}$ nominal complex power;

$\mathbf{V}_{nom}$ load nominal voltage;

$\mathbf{V}$ voltage applied to the load.

In (1), q defines the load type and $q = 0$ is for constant power, $q = 1$ is for the constant current, and $q = 2$ is for the constant impedance.

Mixed loads are modeled by means of a combination of the three load types previously defined in (1), as follows:

$$S = \alpha \cdot \mathbf{S}^{nom} + \delta \cdot \mathbf{S}^{nom} \cdot \left(\frac{|\mathbf{V}|}{|\mathbf{V}_{nom}|} \right) + \beta \cdot \mathbf{S}^{nom} \cdot \left(\frac{|\mathbf{V}|}{|\mathbf{V}_{nom}|} \right)^{2} \tag{2}$$

where

α ratio of the constant power load;

δ ratio of the constant current load;

β ratio of the constant impedance load;

     $\alpha + \beta + \delta = 1.00.$.

D. Distribution Transformer Power Rating

The difficulty in estimating the exact loading of the transformers is one of the error sources in the fault location algorithm. The proposed transformer power rating estimation is performed by using an iterative routine based on (3)

$$\mathbf{S}_i = \left(\lambda_i S_i^{Nom} \cdot \frac{S_{est}}{\sum\limits_{k=1}^{nt} \lambda_k S_k^{Nom}} \right) \cdot [\cos(\varphi_{SS}) + j \sin(\varphi_{SS})] \tag{3}$$

where

S_i^{Nom} transformer apparent power;

S_{est} estimated apparent power;

$\cos(\varphi_{SS})$ measured power factor at the feeder root node;

nt total number of transformers installed on the feeder;

λ_i average loading of the ith transformer.

The apparent power measured at the feeder root node cannot be used directly in (3) because it is composed of demand power and losses. Thus, the estimated power in (3) is calculated in an iterative way. Fig. 2 depicts the procedure employed for estimating the transformer power rating. The load flow method used in the transformer power rating estimation routine is presented in [19]. The variables in Fig. 2 are defined as follows:

$\mathbf{S}_{rn}^{k}$ estimated complex power for the feeder root node in iteration k;

$\mathbf{S}_{rn}^{meas}$ pre-fault complex power measured at the feeder root node;

$\mathbf{S}_{rn}^{calc}$ pre-fault complex power for the feeder root node calculated using power flow phasor quantities in iteration k;

k iteration counter.

The following assumptions are considered regarding Fig. 2:
- initial estimate of the transformer power rating is carried out by means of (3), where $S_{est} = S_{rn}^{meas}$;
- in order to start the load flow, the initial voltage for all nodes is equal to the voltages measured at the feeder root node;
- the convergence is achieved when $\left| \text{Re}\{\mathbf{I}_{rn}^{meas}\} - \text{Re}\{\mathbf{I}_{rn}^{calc}\} \right| \leq \varepsilon$ and
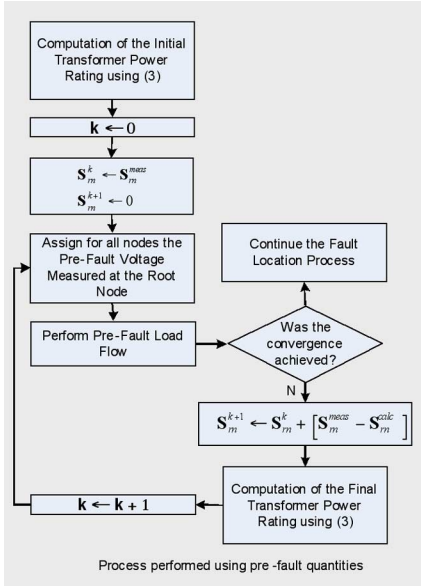
Fig. 2. Transformer power rating estimation.
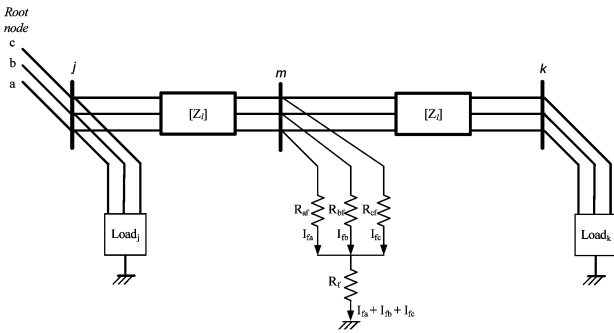
Fig. 3. Distribution line representation.

$\left| \text{Im}\{\mathbf{I}_{rn}^{meas}\} - \text{Im}\{\mathbf{I}_{rn}^{calc}\} \right| \leq \varepsilon$, where ε is a specified tolerance;

- final estimate of the transformer power rating is carried out by means of (3), where $S_{est} = S_{rn}^{k+1}$.

E. Fault Current Computation

Fig. 3 shows a distribution line with loads connected at nodes j and k, and a three-phase fault at node m. Nodal voltages and load currents as well as the total during-fault current measured at the feeder root node are considered to be known during the fault location algorithm computation.

At each iteration of the algorithm, the fault current is computed as follows:

$$\mathbf{I}_f = \mathbf{I}_{rn}^{df,meas} - \sum_{i=1}^{nt} \mathbf{I}_i \qquad (4)$$

where

$\mathbf{I}_{rn}^{df,meas}$ total during-fault current measured at the feeder root node;

I_i load current of the ith transformer;

nt total number of transformers installed on the feeder.
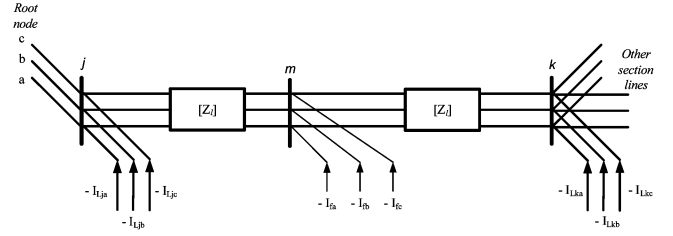
Fig. 4. Current injections at nodes with loads and at the analyzed node.

In the proposed algorithm, a fault is handled as a load connected to the feeder. In each iteration, the fault current calculated using (4) is injected at the analyzed node, as shown in Fig. 4. The usage of current injection does not require any assumption related to the fault impedance, since it does not play a role in the fault modeling.

F. During-Fault Load Flow

The load flow method presented in [19] considers the feeder root node as a reference node, and voltages for this node are known. The initial voltage of all nodes in the fault location algorithm is set as the during-fault voltage phasors measured at the feeder root node. The iterative load flow algorithm steps for radial distribution feeders are as follows.

1) Calculate the load current at each node.
2) Perform a backward sweep for calculating the branch currents. It is carried out starting from the end sections of the last laterals and moving toward the feeder root node.
3) Perform a forward sweep for updating all nodal voltages. It is carried out starting from the feeder root node and moving toward the last sections of the laterals.

Since the three steps described before are executed within one iteration, the convergence is checked.

In [19], the equations for calculating the current injections and the equations for checking the convergence were derived considering only loads of constant power. Since the fault location algorithm must be able to handle loads with changing power in a suitable way, those equations must be defined again. Based on (2), the equations for calculating the current injections are defined in (5), and the equations for checking the convergence are defined in (6), as shown in (5)–(6) at the bottom of the next page, where

$\mathbf{S}$ complex power calculated according to Section IV-D;

$\mathbf{Y}$ shunt admittance;

j feeder node;

n load flow iteration index.

G. Selection of the Likely Fault Location

The selection of the likely fault location is carried out by considering all analyzed nodes during the fault location process. For each analyzed node, the mismatches between calculated during-fault voltage sags and measured during-fault voltage sags are computed. The voltage mismatch, for each faulted phase, is given by

$$\delta_k^{i,j} = V_{k,med}^i - V_{k,sim}^{i,j} \qquad (7)$$

where

$V_{k,med}^{i}$ magnitude of the during-fault voltage sag, on phase k, measured at node i;

$V_{k,sim}^{i,j}$ magnitude of the during-fault voltage sag, on phase k, at node i calculated for a fault at node j.

Equation (7) provides three voltage mismatches for three-phase faults, two voltage mismatches for line-to-line faults, and one voltage mismatch for single-line-to-ground fault. Only the mismatches for the faulted phases are calculated in order to reduce the amount of information handled by the algorithm for asymmetric faults and to ensure that the faulted node is selected based on voltage sags (i.e., the experimented voltage swells on healthy phases for asymmetric faults will not play a role in the final results). In ideal conditions, the voltage mismatches for the faulted node should be zero. In real conditions, the voltage mismatches for the faulted node could not be zero but the magnitudes are almost the same. On the other hand, in some cases, the voltage mismatches for nonfaulted nodes could be smaller than the ones for the faulted node, but, in general, the magnitudes are not the same. Taking into account the previous explanation and the fact that the amount of voltage mismatches is proportional to the fault type, the number of analyzed nodes and the quantity of voltage measurement nodes, it is suitable that the voltage mismatches be represented by only one index for each analyzed node. Thus, the fault location index η is defined by

$$\eta_j = \frac{1.0}{\max\left[\max\left(\delta_k^{i,j}\right) - \min\left(\delta_k^{i,j}\right)\right] + \Delta}$$
$$i = 1, \ldots, mp$$
$$j = 1, \ldots, mn \tag{8}$$

where:

k phase a, b, or c;

mp quantity of voltage measurement nodes used for fault location purposes;

mn number of analyzed nodes;

Δ small number in order to avoid division by zero.

In (8), the term $\max\left[\max\left(\delta_k^{i,j}\right) - \min\left(\delta_k^{i,j}\right)\right]$ ensures that for each analyzed node, among the differences calculated for the phases, the biggest one is chosen. Choosing the biggest difference ensures that the likely faulted node presents the smallest difference among the biggest differences selected. Thus, the fault location index calculated for the faulted node, by means (8), will have the highest value among the analyzed nodes.

The total of η_j given by (8) is equal to the amount of analyzed nodes. The faulted area is defined by means of a ranking established by a decreasing ordering of the fault location index for all analyzed nodes. The likely faulted node is the one represented by the biggest fault location index.

H. Convergence Criterion

The analysis of each analyzed node is performed in an iterative way and the convergence of the algorithm is achieved when the following conditions imposed by (9) are satisfied:

$$\left|\text{Re}\left\{\mathbf{I}_{rn}^{df,meas}\right\} - \text{Re}\left\{\mathbf{I}_{rn}^{df,calc}\right\}\right| \leq \varepsilon$$
$$\left|\text{Im}\left\{\mathbf{I}_{rn}^{df,meas}\right\} - \text{Im}\left\{\mathbf{I}_{rn}^{df,calc}\right\}\right| \leq \varepsilon \tag{9}$$

where

$\mathbf{I}_{rn}^{df,meas}$ total during-fault current measured at the feeder root node;

$\mathbf{I}_{rn}^{df,calc}$ total during-fault current calculated for the feeder root node;

ε specified tolerance.

V. SIMULATION RESULTS

A. Test Feeder

The overhead, three-phase, three-wire, 13.8 kV, 134-node, real-life feeder with a total installed power of 7.065 MVA, shown in Fig. 5, was used for assessing performance of the proposed fault location algorithm. This feeder contains several

$$\begin{bmatrix} \mathbf{I}_{ja} \\ \mathbf{I}_{jb} \\ \mathbf{I}_{jc} \end{bmatrix} = \begin{bmatrix} \left(\frac{\mathbf{S}_{ja}}{\mathbf{V}_{ja}^{(n-1)}}\right)^* & \left(\frac{(\mathbf{S}_{ja})^*}{|\mathbf{V}_{nom}|} \cdot \frac{\mathbf{V}_{ja}^{(n-1)}}{|\mathbf{V}_{ja}^{(n-1)}|}\right) & \left(\frac{\mathbf{V}_{ja}^{(n-1)} \cdot \mathbf{S}_{ja}}{|\mathbf{V}_{nom}|^2}\right) \\ \left(\frac{\mathbf{S}_{jb}}{\mathbf{V}_{jb}^{(n-1)}}\right)^* & \left(\frac{(\mathbf{S}_{jb})^*}{|\mathbf{V}_{nom}|} \cdot \frac{\mathbf{V}_{jb}^{(n-1)}}{|\mathbf{V}_{jb}^{(n-1)}|}\right) & \left(\frac{\mathbf{V}_{jb}^{(n-1)} \cdot \mathbf{S}_{jb}}{|\mathbf{V}_{nom}|^2}\right) \\ \left(\frac{\mathbf{S}_{jc}}{\mathbf{V}_{jc}^{(n-1)}}\right)^* & \left(\frac{(\mathbf{S}_{jc})^*}{|\mathbf{V}_{nom}|} \cdot \frac{\mathbf{V}_{jc}^{(n-1)}}{|\mathbf{V}_{jc}^{(n-1)}|}\right) & \left(\frac{\mathbf{V}_{jc}^{(n-1)} \cdot \mathbf{S}_{jc}}{|\mathbf{V}_{nom}|^2}\right) \end{bmatrix} \cdot \begin{bmatrix} \alpha \\ \delta \\ \beta \end{bmatrix} - \begin{bmatrix} \mathbf{Y}_{ja} & 0 & 0 \\ 0 & \mathbf{Y}_{jb} & 0 \\ 0 & 0 & \mathbf{Y}_{jc} \end{bmatrix} \cdot \begin{bmatrix} \mathbf{V}_{ja} \\ \mathbf{V}_{jb} \\ \mathbf{V}_{jc} \end{bmatrix}^{(n-1)} \tag{5}$$

$$\begin{bmatrix} \Delta\mathbf{S}_{ja}^{(n)} \\ \Delta\mathbf{S}_{jb}^{(n)} \\ \Delta\mathbf{S}_{jc}^{(n)} \end{bmatrix} = \begin{bmatrix} \mathbf{V}_{ja}^{(n)} \cdot \left(\mathbf{I}_{ja}^{(n)}\right)^* \\ \mathbf{V}_{jb}^{(n)} \cdot \left(\mathbf{I}_{jb}^{(n)}\right)^* \\ \mathbf{V}_{jc}^{(n)} \cdot \left(\mathbf{I}_{jc}^{(n)}\right)^* \end{bmatrix} - \begin{bmatrix} \mathbf{Y}_{ja} \cdot |\mathbf{V}_{ja}^{(n)}|^2 \\ \mathbf{Y}_{jb} \cdot |\mathbf{V}_{jb}^{(n)}|^2 \\ \mathbf{Y}_{jc} \cdot |\mathbf{V}_{jc}^{(n)}|^2 \end{bmatrix} - \begin{bmatrix} \mathbf{S}_{ja} & \frac{\mathbf{S}_{ja} \cdot |\mathbf{V}_{ja}^{(n)}|}{|\mathbf{V}_{nom}|} & \mathbf{S}_{ja} \cdot \left(\frac{|\mathbf{V}_{ja}^{(n)}|}{|\mathbf{V}_{nom}|}\right)^2 \\ \mathbf{S}_{jb} & \frac{\mathbf{S}_{jb} \cdot |\mathbf{V}_{jb}^{(n)}|}{|\mathbf{V}_{nom}|} & \mathbf{S}_{jb} \cdot \left(\frac{|\mathbf{V}_{jb}^{(n)}|}{|\mathbf{V}_{nom}|}\right)^2 \\ \mathbf{S}_{jc} & \frac{\mathbf{S}_{jc} \cdot |\mathbf{V}_{jc}^{(n)}|}{|\mathbf{V}_{nom}|} & \mathbf{S}_{jb} \cdot \left(\frac{|\mathbf{V}_{jb}^{(n)}|}{|\mathbf{V}_{nom}|}\right)^2 \end{bmatrix} \cdot \begin{bmatrix} \alpha \\ \delta \\ \beta \end{bmatrix} \tag{6}$$
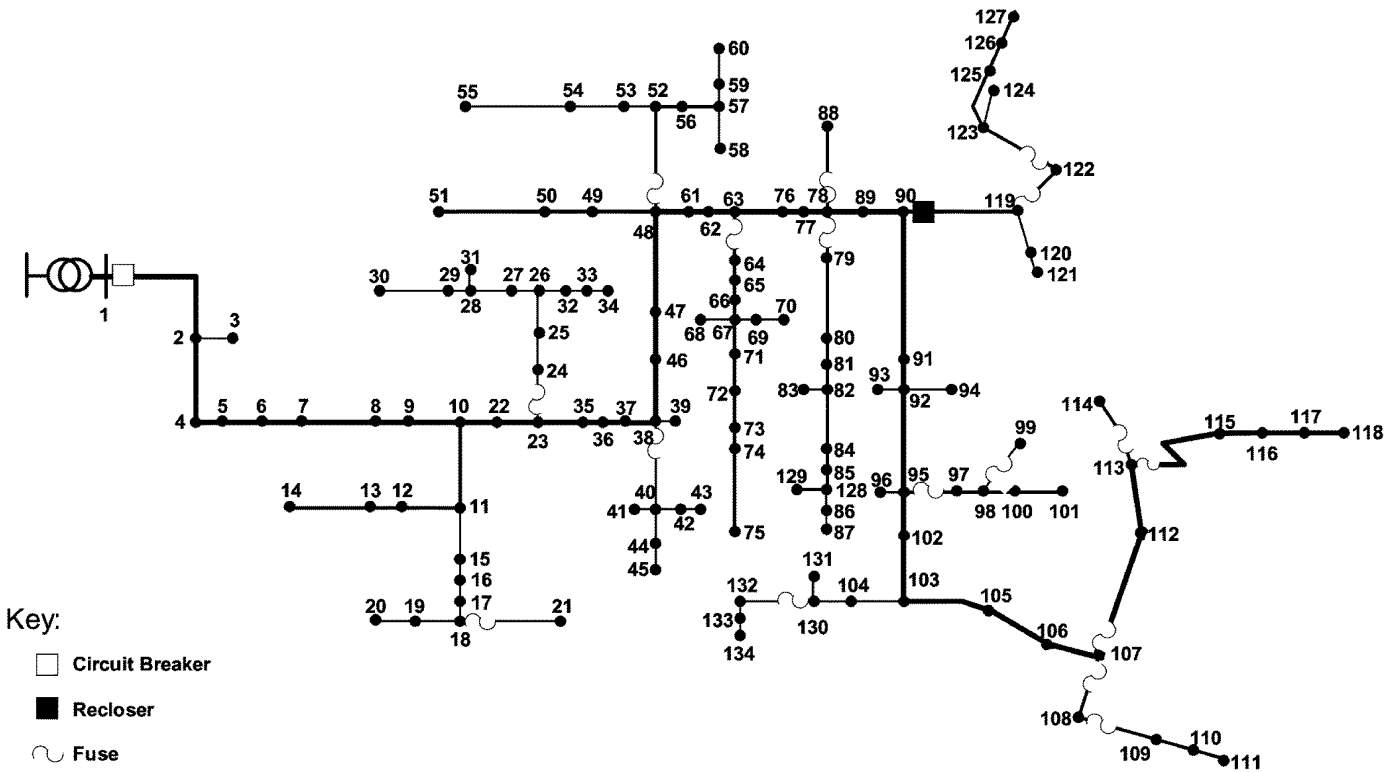
Fig. 5. Real-life feeder used for evaluating the fault location algorithm.

laterals, and the furthest node is located 4270.0 m from the substation.

B. Remote Sparse Measurements

Fault location was performed considering four voltage sag measurement devices placed along the feeder. These measurement devices were placed at nodes 20, 81, 115, and 125.

C. Effectiveness Assessment of the Fault Location Algorithm

Several tests were carried out in order to evaluate the effectiveness of the fault location algorithm. For this purpose, faults were simulated at all nodes using the ATP program [20] with loads modeled as constant impedances. Several values for fault resistances were used. The constant impedance model and the same transformer power ratings used in ATP simulations were employed in the fault location algorithm. As single phase-to-ground faults occur more frequently, only this type of fault is analyzed. Results for two tests regarding single line-to-ground faults at phase A are presented. The fault location algorithm has achieved 100% of accuracy (i.e., the faulted node was indicated in the first position of the fault location ranking by the algorithm), for the tests using fault resistances of 0.1 Ω and 25.0 Ω. Fig. 6 shows the during-fault voltage magnitude calculated for the faulted node by the ATP for a fault resistance of 0.1 Ω as well as the during-fault voltage magnitude computed by the algorithm.

Fig. 7 shows the during-fault voltage magnitude calculated for the faulted node by the ATP for a fault resistance of 25.0 Ω
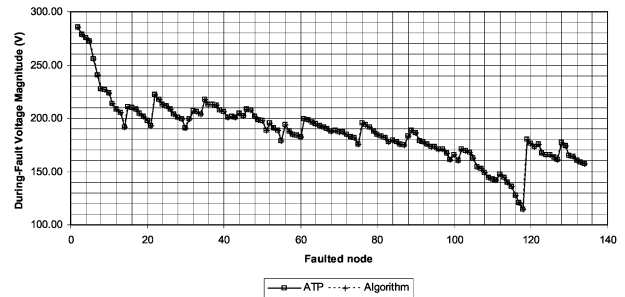
Fig. 6. During-fault voltage magnitude calculated for the faulted node by ATP and by the algorithm for faults with a fault resistance of 0.1 Ω.
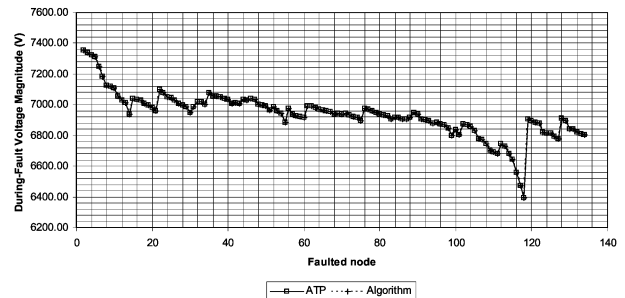
Fig. 7. During-fault voltage magnitude calculated for the faulted node by ATP and by the algorithm for faults with a fault resistance of 25.0 Ω.

as well as the during-fault voltage magnitude computed by the algorithm.

The calculated magnitudes by the algorithm are practically the same magnitudes computed by the ATP program as shown in Figs. 6 and 7. Thus, the effectiveness of the fault location is
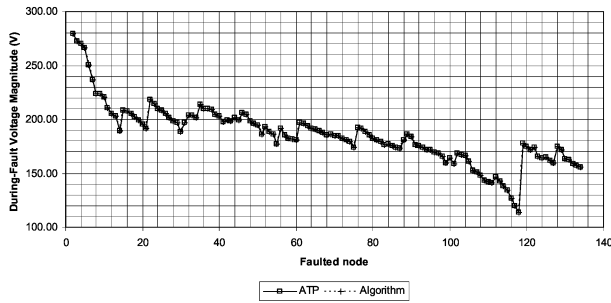
Fig. 8. During-fault voltage magnitude calculated for the faulted node by ATP and by the algorithm for faults with a fault impedance of $0.0 + j0.1\ \Omega$.
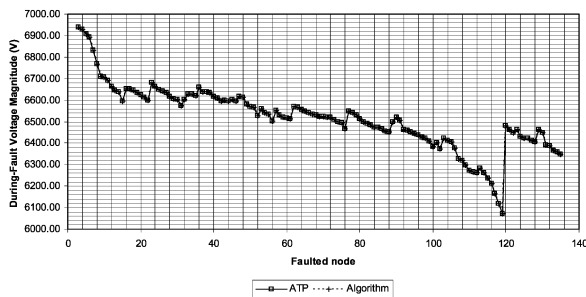
Fig. 9. During-fault voltage magnitude calculated for the faulted node by ATP and by the algorithm for faults with a fault impedance of $0.0 + j25.0\ \Omega$.
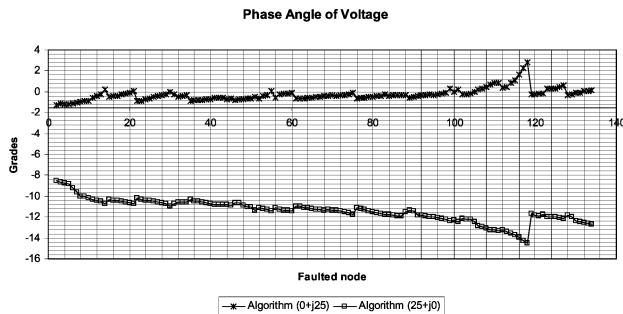
Fig. 10. Phase angle of the during-fault voltage calculated for the faulted node by the algorithm for faults with a fault impedance of $25.0 + j0.0\Omega$ and $0.0 + j25.0\Omega$.

ensured once the same effects that occurred in a fault are reproduced by the algorithm.

D. Assessment of Impedance Independence of the Algorithm

It is known that some fault location approaches are derived under the hypothesis that the fault impedance is purely resistive. In the last paragraph of section I and in Section IV-E, it is stated that no fault impedance is required in the fault modeling used in the algorithm. Several tests were carried out by using different fault impedances in order to assess the algorithm independence of the fault impedance and to ensure that the algorithm is immune to the composition of the fault impedance. For this purposes, single line-to-ground faults (phase A) were simulated, at all nodes, using loads modeled as constant impedances in the ATP simulations. In the fault location algorithm, the same constant impedance model along with the same transformer power ratings as the ones employed in ATP simulations

were used. The fault location algorithm has achieved 100% accuracy. The faulted node was indicated in the first position of the fault location ranking by the algorithm, for the tests using fault impedances of $0.0 + j0.1\ \Omega$ and $0.0 + j25.0\ \Omega$. Figs. 8 and 9 present the during-fault voltage magnitudes calculated by ATP and by the algorithm for faults with the aforementioned fault impedances.

These figures show that the calculated magnitudes by the algorithm are practically the same magnitudes computed by the ATP program. Additionally, the during-fault voltage magnitudes shown in the figures of Section V-C are very similar to the magnitudes shown in the figures of this subsection. The main difference among quantities of both subsections is related to the phase angle. Fig. 10 shows the phase angle of during-fault voltages, which were computed by the algorithm as shown in Figs. 8 and 9.

Independently of the fault impedance, the fault location algorithm reproduces the same effects of the fault as ATP. Thus, the impedance-independence of the algorithm is ensured.

VI. TESTS OF ACCURACY AND ROBUSTNESS

In order to assess the accuracy and robustness of the algorithm, faults were simulated at several feeder nodes taking into account different transformer loadings, different fault resistances, and different fault types. Since the majority of faults that occur in a feeder are single phase-to-ground faults, the analysis of this type of fault is emphasized. Data generated by means of simulations are used as measured data by the fault location algorithm. Table I presents the parameters used in some simulations carried out with the ATP program. ATP simulations were carried out by taking transformer nominal loadings into account.

A. Modeling of Lines and Loads

Nontransposed distribution lines were modeled as in-series RL, and shunt capacitances were neglected in ATP simulations as well as in the fault location algorithm. In ATP simulations, loads were modeled as constant impedances, and in the fault location algorithm, loads were modeled as described in Section IV-C earlier.

B. Influence of the Load Model on the Algorithm

As previously mentioned in Section V-C, ATP simulations use the constant impedance load model. Aiming at evaluating the algorithm robustness against variations between the load model used in ATP simulations and the one used in the algorithm, six load combinations were used for representing loads connected to the feeder. These combinations are defined according to (2) and their parameters are presented in Table II.

In Fig. 5, all nodes were analyzed during the fault location process for each fault indicated in Table I. In the fault location process, the transformer power rating was estimated as detailed in Section IV-D earlier and the average loading was equal to the nominal power [i.e., $\lambda = 1.0$ in (3)]. Errors were not verified for locating single-line-to-ground faults at nodes 55, 105, 113, and 134, because the pointed nodes exactly match with the faulted node. Table III shows the maximum deviation in the distance

TABLE I
ATP SIMULATION PARAMETERS

Node	Fault type	Fault Resistance (Ω)			
		R_f	R_{af}	R_{bf}	R_{cf}
15; 25; 36; 40; 55; 85; 105; 113; 126; 134	AN	1.0; 5.0; 10.0; 15.0; 20.0; 25.0	-	-	-
113; 126	BCN	5.0	-	0.1	0.1
15; 105	ABC	-	1.0	1.0	1.0

TABLE II
PARAMETERS OF THE LOAD COMBINATIONS USED
IN THE FAULT LOCATION ALGORITHM

Parameter/Load Combination	LC1	LC2	LC3	LC4	LC5	LC6
α	0.00	0.00	0.00	0.00	0.00	0.15
β	1.00	0.75	0.50	0.25	0.00	0.60
δ	0.00	0.25	0.50	0.75	1.00	0.25
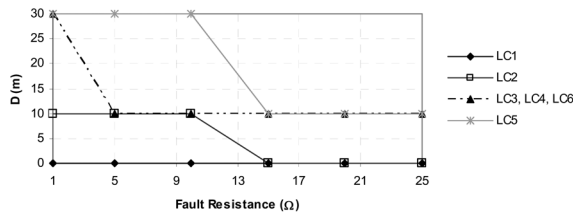
Fig. 11. Distance between node 15 and the node pointed by the algorithm.

Fig. 12. Distance between node 40 and the node pointed by the algorithm.

TABLE III
MAXIMUM DEVIATION IN THE DISTANCE OBSERVED FOR LOCATING FAULTS
FOR NODES 25, 36, 85, AND 126 ALONG WITH THE LOAD COMBINATION
AND FAULT RESISTANCE USED FOR SIMULATING FAULTS IN ATP

Node	Maximum Deviation in the Distance (m)	Load Combination	Fault Resistance (Ω)
25	140.0	LC4; LC5; LC6	1.0
36	70.0	LC5; LC6	1.0
85	70.0	LC2; LC3; LC4; LC5; LC6	1.0; 5.0; 10.0; 15.0; 20.0; 25.0
126	40.0	LC2; LC3; LC4; LC5; LC6	1.0; 5.0; 10.0; 15.0; 20.0; 25.0

(D) between the faulted node and the node pointed by the algorithm for faults at nodes 25, 36, 85, and 126. Figs. 11 and 12 show the distance (D), in meters, between the faulted node and the node pointed by the algorithm for single-line-to-ground at nodes 15 and 40.

As shown in Table III as well as Figs. 11 and 12, the biggest distance between the faulted node and the node pointed by the algorithm is 140 m, and in most cases, the distance is smaller than 100 m. These errors are quite acceptable due to the faulted
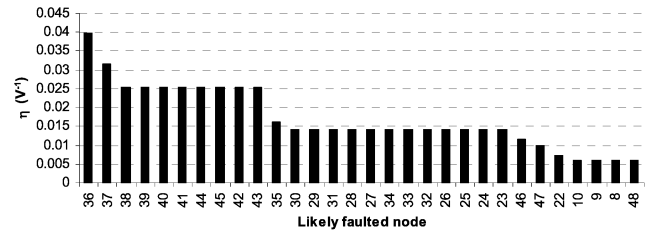
Fig. 13. First 30 positions of the ranking nodes for a single-line-to-ground fault location at node 40.
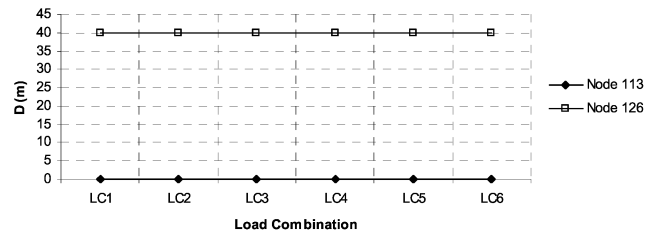
Fig. 14. Distance between the faulted node and the node pointed by the algorithm for double line-to-ground faults at nodes 113 and 126.
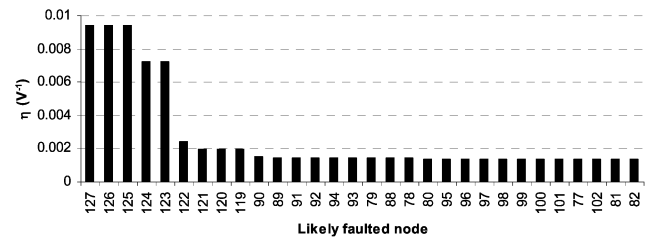
Fig. 15. First 30 positions of the ranking nodes for a double line-to-ground fault location at node 126.

node always being presented at the first position in the faulted nodes ranking. Fig. 13 illustrates the ranking given by the algorithm using the load combination LC5 for locating a single-line-to-ground fault at node 40. The fault resistance is equal to 1.0 Ω.

Fig. 13 shows that for some nodes, the fault location indices keep constant. Thus, areas containing the likely faulted node can be established. These areas provide the maintenance crew with enough information for minimizing the time for fault location, network repairs, and restoration of the power supply.

Fig. 14 shows the distance (D) for locating a double line-to-ground fault at nodes 113 and 126. Fig. 15 shows the faulted nodes ranking given by the algorithm for locating the fault at node 126. The load combination LC6 was used.

In Fig. 15, the faulted node appears in the second position of the ranking. The node at the first position of the ranking is 40 m away from node 126. Therefore, this result is very reliable for fault location purposes.

The distance (D) for fault location of a three-phase fault at nodes 15 and 105 is shown in Fig. 16. The faulted node ranking given by the algorithm for locating the fault at node 15, using the load combination LC4, is shown in Fig. 17.

In Fig. 17, the faulted node is ranked in the second position and the node of the first position of the ranking is 10 m away from node 15. Again, this result is very reliable for fault location purposes.
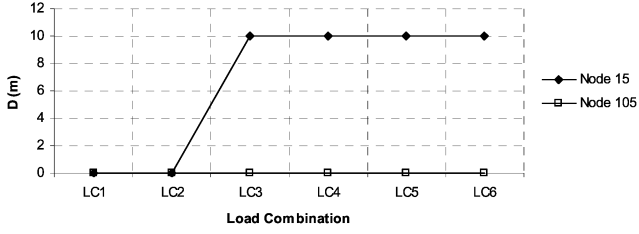
Fig. 16. Distance between the faulted node and the node pointed by the algorithm for three-phase faults at nodes 15 and 105.
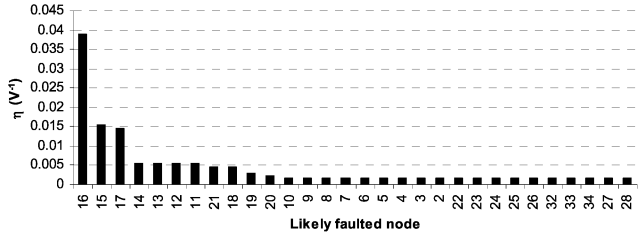
Fig. 17. First 30 positions of the ranking nodes for a three-phase fault location at node 15.

C. Influence of the Transformer Loading Uncertainness in the Algorithm

The fault location algorithm estimates the transformer power rating using the procedure presented in Section IV-D earlier. Each transformer has the same percentage of loading of its nominal power. Due to the customer behavior uncertainties, the transformer loadings have a stochastic behavior. Several transformers in the feeder may have different loadings when a fault occurs. Aiming at assessing the influence of the uncertainness of the transformer loading, ATP simulations were carried out by taking into account random loading for each transformer. In order to accomplish it, a variable ξ with a normal distribution, mean one, and standard deviation σ was randomly selected. Thus, the complex power of each transformer used in the ATP simulations is given by

$$\mathbf{S}_i^{ATP} = \xi_i \cdot S_i^{Nom} \cdot (\cos \varphi + j \sin \varphi) \qquad (10)$$

where

ξ_i	random variable of a normal distribution, mean one, and standard deviation σ;
S_i^{Nom}	nominal apparent power of the ith transformer;
$\cos \varphi$	power factor equal to 0.92.

According to (10) for the ith transformer, the difference between the nominal apparent power and the loading used in ATP simulations increases when the standard deviation σ is increased. Six different standard deviations were used in ATP simulations for faults at nodes 40 and 105. The variable ξ randomly selected from a normal distribution of mean one and standard deviation equal to 0.2, 0.6, and 1.0 is shown in Fig. 18. Different values of fault resistance were used in the ATP simulations. The transformer power rating in the fault location algorithm was estimated as described in Section IV-D earlier with $\lambda = 1.0$ in (3), and the load combination LC1
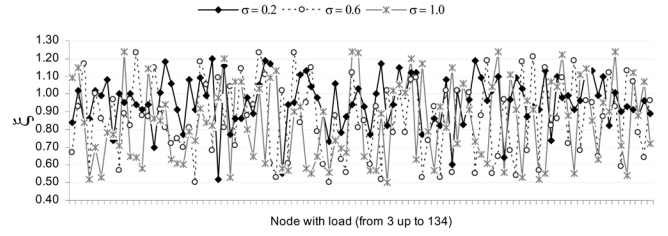
Fig. 18. Random variable ξ for $\sigma = 0.2$, 0.6, and 1.0.
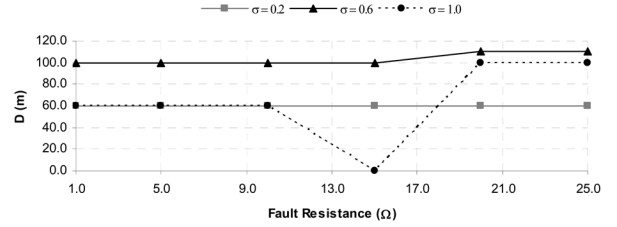
Fig. 19. Distance between the faulted node and node pointed by the algorithm for faults at node 40.
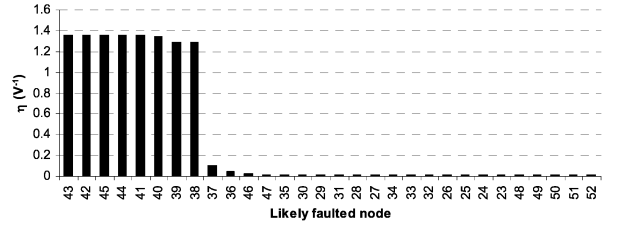
Fig. 20. Ranking of the likely faulted nodes for a single-line-to-ground fault simulated at node 40 with a fault resistance of 1.0 Ω, ξ with mean one and $\sigma = 0.2$.

was used. For a fault at node 105, the algorithm points to the faulted node. For the fault location at node 40, the distance (D) is shown in Fig. 19.

The rankings of the fault location indices for locating three single-line-to-ground faults are shown in Figs. 20–22. Fig. 20 shows the fault location results for a fault simulated using the fault resistance being equal to 1.0 Ω and, ξ with mean one and $\sigma = 0.2$. The results provided by the algorithm are reliable because the pointed faulted node is 60 m away from the actual faulted node. Besides, all nodes from the first to the sixth position of the ranking are enclosed within a geographical area protected by a fuse. It ensures the applicability, robustness, and reliability of the fault location algorithm.

In Fig. 21, the fault was simulated with a fault resistance of 25.0 Ω, ξ with mean one and $\sigma = 0.6$. In this case, the actual faulted node is ranked at the fourth position and it is 110 m away from node 37 ranked at the first position. Even for this error of more than 100 m, the algorithm gives good quality results because the first nine positions of the ranking belong to the same geographical area. This fault could be located by using the algorithm results along with the information that the fault was cleared by a fuse and not by the circuit breaker placed at the feeder root node.

In Fig. 22, the fault was simulated with a fault resistance of 20.0 Ω, ξ with mean one, and $\sigma = 1.0$. In this case, the actual faulted node is ranked at the third position and it is 100 m away from node 38 ranked at the first position. The fault location error
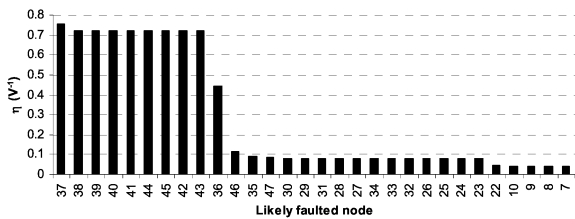
Fig. 21. Ranking of the likely faulted nodes for a single-line-to-ground fault simulated at node 40 with a fault resistance of 25.0 Ω, ξ with mean one and $\sigma = 0.6$.
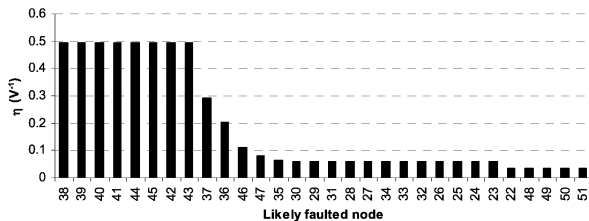
Fig. 22. Ranking of the likely faulted nodes for a single-line-to-ground fault simulated at node 40 with a fault resistance of 20.0 Ω, ξ with mean one and $\sigma = 1.0$.

is 100 m. Even for this error, the algorithm provides good quality results because the fault could be located by using the algorithm results along with information related to the fault clearing.

D. General Comments Regarding the Results

From the previous results, it is intuitive that the bigger the number of measurement nodes are, the better the accuracy of the algorithm is. The accuracy increases until a certain number of measurement nodes is reached, which is defined basically by the feeder characteristics, such as topology, load level, amount of lateral branches, and load taps. After this point, the increasing measurement nodes will only guarantee the redundancy of the measurements but may not contribute to an increase in accuracy. Analyzing the presented fault location rankings obtained by using four measurement nodes, the fault location indices are almost the same for many nodes. Thus, the accuracy of the algorithm could be improved by means of increasing the number of measurement nodes, but this may be unacceptable due to either technical or economical constraints. The best way to improve the algorithm accuracy without increasing the number of measurement nodes is to use optimization modeling, for placement of the measurement devices similar to what was presented in [21] and [22].

VII. Conclusion

A robust and efficient algorithm that uses sparse voltage sag measurements for fault location in electric distribution feeders was proposed. Most utilities can implement this algorithm with some moderate investments. The main requirements are the existence of devices for acquisition, processing, and transmission of voltage and current signals.

Even placing the measurement devices without using optimized modeling, the presented test results ensure that the proposed algorithm is an excellent tool that can aid the fault location process, mainly when the faulted point is at a hidden place on the feeder. Generally, hidden faults are difficult to locate de-

manding a long time to restore the power supply. Often, this situation degrades the reliability indices and can drive away the reliability performance from the required standard.

References

[1] C. A. Warren, "Distribution reliability: What is it?," *IEEE Ind. Appl. Mag.*, vol. 2, no. 4, pp. 32–37, Jul./Aug. 1996.

[2] M. Lehtonen, S. Pettissalo, and J. H. Etula, "Calculational fault location for electrical distribution networks," in *Proc. IEEE 3rd Int. Conf. Power System Monitoring and Control*, 1991, pp. 38–43.

[3] A. A. Girgis and C. M. Fallon, "Fault location techniques for radial and loop transmission systems using digital fault recorded data," *IEEE Trans. Power Del.*, vol. 7, no. 4, pp. 1936–1945, Oct. 1992.

[4] A. A. Girgis, C. M. Fallon, and D. L. Lubkeman, "A fault location technique for rural distribution feeders," *IEEE Trans. Ind. Appl.*, vol. 29, no. 6, pp. 1170–1175, Nov./Dec. 1993.

[5] R. Das, M. S. Sachdev, and T. S. Sidhu, "A fault locator for radial subtransmission and distribution lines," in *Proc. IEEE Power Eng. Soc. Summer Meeting*, 2000, pp. 443–448.

[6] M. Lehtonen, A. Matsinen, E. Antila, J. Kuru, P. Vuorenpaa, E. Matinlassi, and S. Pettissalo, "Automatic fault management in distribution networks," presented at the 16th Int. Conf. Exhibit. Electricity Distribution, Jun. 18–21, 2001, Conf. publ. no. 482.

[7] R. K. Aggarwal, Y. Aslan, and A. T. Johns, "New concept in fault location for overhead distribution systems using superimposed components," *Proc. Inst. Elect. Eng., Gen., Transm. Distrib.*, vol. 144, no. 3, pp. 309–316, May 1997.

[8] J. Zhu, D. L. Lubkeman, and A. A. Girgis, "Automated fault location and diagnosis on electric power distribution feeders," *IEEE Trans. Power Del.*, vol. 12, no. 2, pp. 801–809, Apr. 1997.

[9] S. J. Lee, M. S. Choi, S. H. Kang, B. G. Jin, D. S. Lee, B. S. Ahn, N. S. Yoon, H. Y. Kim, and S. B. Wee, "An intelligent and efficient fault location and diagnosis scheme for radial distribution systems," *IEEE Trans. Power Del.*, vol. 19, no. 2, pp. 524–532, Apr. 2004.

[10] E. C. Senger, G. Manassero, C. Goldemberg, and E. L. Pellini, "Automated fault location system for primary distribution networks," *IEEE Trans. Power Del.*, vol. 20, no. 2, pt. 2, pp. 1332–1340, Apr. 2005.

[11] H. Li, A. S. Mokhar, and N. Jenkins, "Automated fault location on distribution network using voltage sags measurements," presented at the 18th Int. Conf. Exhibit. Electricity Distribution, Turin, Italy, Jun. 6–9, 2005, Session 3.

[12] V. N. Gohokar and M. K. Khedkar, "Faults locations in automated distribution system," *Elect. Power Syst. Res.*, vol. 75, pp. 51–55, 2005.

[13] D. J. Won, I. Y. Chung, J. M. Kim, S. I. Moon, J. C. Seo, and J. W. Choe, "A new algorithm to locate power-quality event source with improved realization of distributed monitoring scheme," *IEEE Trans. Power Del.*, vol. 21, no. 3, pp. 1641–1674, Jul. 2006.

[14] P. Jarventausta, P. Verho, and J. Partenen, "Using fuzzy sets to model the uncertainty in the fault location process of distribution networks," *IEEE Trans. Power Del.*, vol. 9, no. 2, pp. 954–960, Apr. 1994.

[15] Y. Tang, H. F. Wang, R. K. Aggarwal, and A. T. Johns, "Fault indicators in transmission and distribution systems," in *Proc. Int. Conf. Electric Utility Deregulation and Restructuring and Power Technologies, City University*, Apr. 4–7, 2000, pp. 238–243.

[16] S. Luo, M. Kezunovic, and D. R. Sevick, "Locating faults in the transmission network using sparse field measurements, simulation data and genetic algorithm," *Elect. Power Syst. Res.*, vol. 71, no. 2, pp. 169–177, 2004.

[17] A. Abur and Z. Galijasevic, "Fault location using voltage measurements," *IEEE Trans. Power Del.*, vol. 17, no. 2, pp. 441–445, Apr. 2002.

[18] R. A. F. Pereira, L. G. W. da Silva, M. Kezunovic, and J. R. S. Mantovani, "Location of single-line-to-ground faults on distribution feeders using voltage measurements," presented at the Latin America Transmission and Distribution Conf. Expo., Caracas, Venezuela, Aug. 15–18, 2006.

[19] C. S. Cheng and D. Shirmohammadi, "A three-phase power flow method for real-time distribution system analysis," *IEEE Trans. Power Syst.*, vol. 10, no. 2, pp. 671–679, May 1995.

[20] "ATP Rulebook. Comitê Brasileiro de Usuários de EMTP/ATP, Brazil," 1976.
[21] R. A. F. Pereira, L. G. W. da Silva, and J. R. S. Mantovani, "PMUs optimized allocation using a tabu search algorithm for fault location in electric power distribution system," presented at the Latin America Transmission and Distribution Conf. Expo., São Paulo, Brazil, 2004.
[22] R. A. F. Pereira, L. G. W. da Silva, M. Kezunovic, and J. R. S. Mantovani, "Optimized placement of voltage measurement devices for determining location of single line-to-ground faults on overhead electric power distribution feeders," presented at the XVI Automatic Brazilian Congr., Salvador, Brazil, 2006.

Rodrigo Aparecido Fernandes Pereira was born in Adamantina, Brazil, on September 1, 1976. He received the B.Sc., M.S., and Ph.D. degrees in electrical engineering from UNESP/Ilha Solteira, São Paulo, Brazil, in 2001, 2003, and 2007, respectively.

Currently, he is an Associate Researcher in the Electric Power Systems Planning Laboratory at UNESP/Ilha Solteira. His research areas are fault location on distribution feeders and protection and reliability of electric distribution systems.

Luis Gustavo Wesz da Silva received the B.Sc. degree in the electrical engineering from UNIDERP-MS in 1999 and the M.S. and the Ph.D degrees in electrical engineering from UNESP/Ilha Solteira, São Paulo, Brazil, in 2002 and 2005, respectively.

Currently, he is a Fellowship Holder of the Human Resources Fixation Program of CNPq—Brazil in the Electrical Engineering and Computer School at the Federal University of Goiás—Brazil. His research areas are protection of distribution feeders, heuristic algorithms, quality and reliability of the power supply, as well as electric power systems planning.

Mladen Kezunovic (S'77–M'80–SM'85–F'99) received the Dipl.Ing. degree in electrical engineering from the University of Sarajevo, Bosnia-Herzegovina, in 1974, and the M.S. and Ph.D. degrees from the University of Kansas, Lawrence, in 1977 and 1980, respectively.

Currently, he is the Eugene E. Webb Professor and Site Director of Power Engineering Research Center, an National Science Foundation Industry/University Cooperative Research Centers (I/UCRC) at Texas A&M University, College Station. His main interests are digital simulators and simulation methods for relay testing as well as the application of intelligent methods to power system monitoring, control, and protection.

Dr. Kezunovic is a member of CIGRE–Paris.

José Roberto Sanches Mantovani (M'06) received the B.Sc. degree from UNESP/Ilha Solteira, São Paulo, Brazil, in 1981, and the M.S. and Ph.D. degrees in electrical engineering from UNICAMP—Campinas—SP—Brazil, in 1987 and 1995, respectively.

Currently he is an Associate Professor in the Electrical Engineering Department at UNESP/Ilha Solteira. His research areas are planning and control of electric power systems.